STUDY OF AXISYMMETRIC SUBSONIC AND SUPERSONIC FREE JETS

Annika Hell*, Eduard Rosenko*, Bernhard Weigand* and Stefan Schlamp**
*Institut für Thermodynamik der Luft- und Raumfahrt (ITLR), Universität Stuttgart
**Department of Mechanical and Process Engineering, ETH Zürich

ABSTRACT
To provide experimental reference cases for the investigation of supersonic combustion, we investigated subsonic and supersonic axisymmetric free jets at matched conditions using the continuously operating supersonic combustion facility at the ITLR.
Three different free jets with total temperatures of up to 550 K were surveyed by conventional probe measurement (pitot pressure, total temperature) and the nonintrusive, seedless, nonlinear, laser based technique Laser-Induced Thermal Acoustics (LITA). LITA allows measuring the local speed of sound in a test volume. The uncertainties are about 2.2 %.
Speed of sound and static temperature profiles are presented and discussed. Additional a commercial CFD code was used to simulate the flow. Good agreement between the different measurement techniques and the numerical simulation was found.

INTRODUCTION

For scramjet development the understanding of supersonic combustion is essential. In addition, the development is complicated by the fact that none of the current ground test facilities are capable of perfectly reproducing the flight conditions of a real combustor. Thus computational fluid dynamics (CFD) codes, which are used to analyze high speed flows, fuel-air mixing and combustion, are an important component of the development. For the validation of the CFD codes experimental test cases and data are necessary.
A basic validation case is an axisymmetric free jet emanating from a nozzle. First experimental investigations concentrated on unheated supersonic free jets of air. Eggers [1] investigated a free jet produced by a Ma = 2.2 convergent-divergent nozzle. He surveyed the total pressure across the jet at various axial locations from the nozzle exit plane downstream to 75 nozzle diameter. Even though the jet was not pressure matched and shock structures in the jet developed, the experimental results are used as validation case. At the NASA Lewis research center Panda et al. [2],[3] measured the flow field (axial component of velocity and temperature) of unheated subsonic and supersonic free jets downstream of convergent and convergent-divergent nozzles, respectively. With a Rayleigh scattering-based technique, investigations of shock structures [2] and measurements of the velocity and density fluctuations [3] were also possible.
As additional validation cases we investigated an unheated (T_0 = 292 K) subsonic free jet and unheated and heated (T_0 = 550 K) supersonic free jets. The experiments were conducted at the supersonic combustion facility of the Institut für Thermodynamik der Luft- und Raumfahrt (ITLR). The free jets were investigated using a conventional probe measurement (wall pressure distribution, pitot pressure, total temperature) and by the laser based technique Laser-Induced Thermal Acoustics (LITA). The results were compared to CFD predictions.

Additional to the investigation of a free jet we concentrated on the comparison of different measurement techniques, in order to verify the use of LITA in highly turbulent compressible flows. Probe measurements are limited to non reacting flows at moderate total temperatures up to T_0 = 550 K. Therefore the investigation of burning free jets, which we plan in future, requires the use of nonintrusive laser measurement techniques such as LITA. After giving an overview of the experimental setup, the results of subsonic and supersonic test cases will be presented.

EXPERIMENTAL SETUP

Test Facility

The supersonic combustion facility at ITLR is a continuously operating facility (see Figure 1). It consists of a 600 kW screw compressor fed by atmospheric air. The compressed air moves through a two-stage, electric heater with a total electrical power consumption of 1 MW. The facility can deliver a flow with a maximum

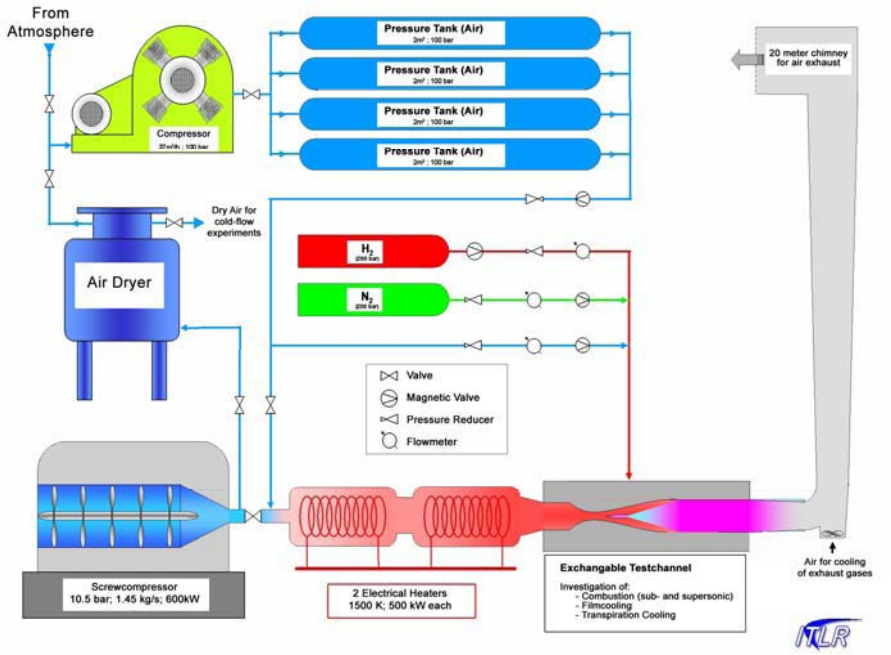

Figure 1: Supersonic test facility

total temperature of T_{max} = 1500 K and a maximum mass flow rate of $\dot{m}$ = 1.45 kg/s at a maximum total pressure of p_{max} = 10 bar. The heated air is led in the test section where various test sections can be mounted, e.g. combustion chamber, film cooling channel and nozzles for free jet generation. The used subsonic nozzle and the supersonic nozzle are shown in Figure 2 and Figure 3, respectively. In both nozzles a thermocouple is located in the nozzle plenum to measure the total temperature.

The subsonic nozzle is a perspex model of the outer nozzle contour used at the ITLR to produce supersonic reacting free jets. The nozzle is convergent-divergent and at the end a section with constant diameter is attached. This section is originally used to enhance mixing processes. The left red line indicates the nozzle throat and the line further downstream marks the beginning of constant cross-section. As the nozzle is made of perspex we investigated only unheated flows at ambient temperature. 32 wall pressure holes are arranged in the nozzle wall.

The supersonic nozzle is a purpose made, convergent-divergent, stainless steel nozzle to investigate heated air jets. The nozzle is cooled at the mounting area to the supersonic combustion facility. At the design pressure ratio p_∞/p_0 = 0.2724 a supersonic free jet of Ma ≈ 1.5 is produced. For the inviscid contour

design the method of characteristics according to Prandtl and Busemann [4] was used. The contour was corrected by the absolute value of the displacement thickness obtained by a boundary layer calculation.

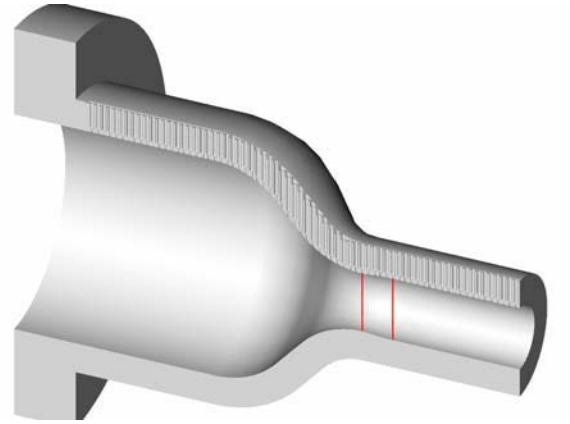

Figure 2: Subsonic Nozzle

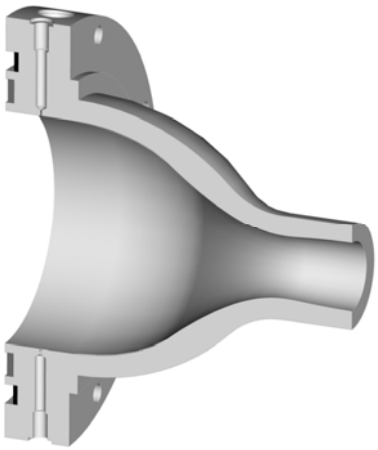

Figure 3: Supersonic nozzle

Measurement Technique

In this work we compare conventional intrusive probe measurements with LITA. To measure at different locations in the free jet, the probes and the optical LITA setup were mounted on a computer controlled three-axis translation table. The probe tips are cylindrical and cut square, with outside and inside diameters for the pitot probe of 5 mm and 2 mm, respectively and for the total temperature probe 5 mm and 3.5 mm, respectively. Errors in pitot pressure due to pressure transducer errors are ±1 % (here: ±0.07 bar). Measurement uncertainty of the total temperature due to thermocouple uncertainty is ±2 K.

LITA allows measuring the local speed of sound, the flow velocity and gas composition in a test volume. It has been developed by Cummings [5],[6], who measured the speed of sound. Schlamp continued the work and extended LITA for measuring flow velocity [7] and gas composition [8]. In this work the local speed of sound is measured. The uncertainty for the speed of sound measurement is less than 2.2%.

Since the gas composition is known the static temperature can be calculated. A schematic drawing of the optical setup is presented in Figure 4.

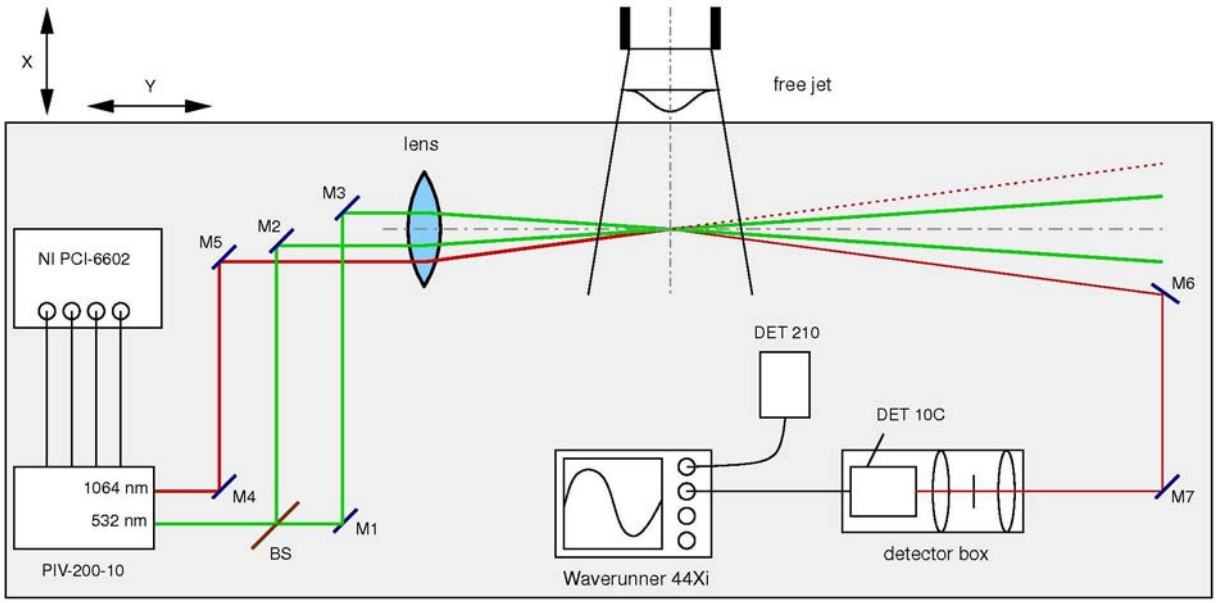

Figure 4: Schematic drawing of the LITA Setup

LITA is based on the effect of electrostriction and requires two laser beams. As source beam we used a dual-cavity pulsed Nd:YAG laser (Spectra Physics, PIV-200-10). One laser beam is frequency doubled (λ_{exc} = 532 nm, pulse width = 10 ns) and provides an excitation pulse, which is split by a beam splitter (BS). The split laser beams are parallel aligned by a mirror system (M1 – M3) and are focused by a lens (focal length = 1000 mm). Thus an electric field intensity grating is induced in the focal point of the lens. The intensity grating polarizes the molecules, which are then accelerated to the intensity maxima and minima. Due to the acceleration a velocity grating is produced that induces a density grating. A second laser beam (λ_{int} = 1064 nm, pulse width = 10 ns) is used to interrogate the density grating over time by varying the delay between both pulses from shot to shot. The timing of the two laser cavities is performed by a computer controlled timer board (National Instruments, PCI 6602). The interrogation beam is directed by mirror M4 and M5 to the lens and focused on the test volume. Due to the density grating a fraction of the beam is reflected. This reflected beam is the signal beam and is directed by mirror M6 and M7 into the detector box. The beam is spatially filtered (50 µm pin hole) and detected by a photo detector (Thorlabs, DET 10C). The signal is amplified (Hamamatsu, C 5594) and recorded by a digital storage oscilloscope (LeCroy, Waverunner 44Xi). The recorded signal has the shape of a damped oscillation, whose frequency is proportional to the speed of sound.

NUMERICAL INVESTIGATION

In addition to the experiments, numerical simulations of the nozzle flow and the free jets were performed. The calculations were done by the commercial, finite-volume CFD code FLUENT™ 6.3, assuming an axisymmetric flow of thermally perfect gases. The calculations are steady and compressible. Turbulence is modeled with a k-ε model. The convection and diffusion terms in the discretized scalar transport equation are solved using a second-order upwind scheme. Inviscid fluxes are calculated using the Roe flux-difference splitting.
Structured grids, generated by the commercial code GAMBIT™ are used for the calculation. Near the nozzle walls the grid points are clustered to resolve the boundary layer. The dimensionless distance between the wall inside the nozzle and first cell center is less than $y_1^+ = 1$. The grid consists of 155,000 cells and 129,450 cells for subsonic and supersonic free jet, respectively. The complete mesh and the mesh within the range of the subsonic nozzle exit are shown in Figure 5.

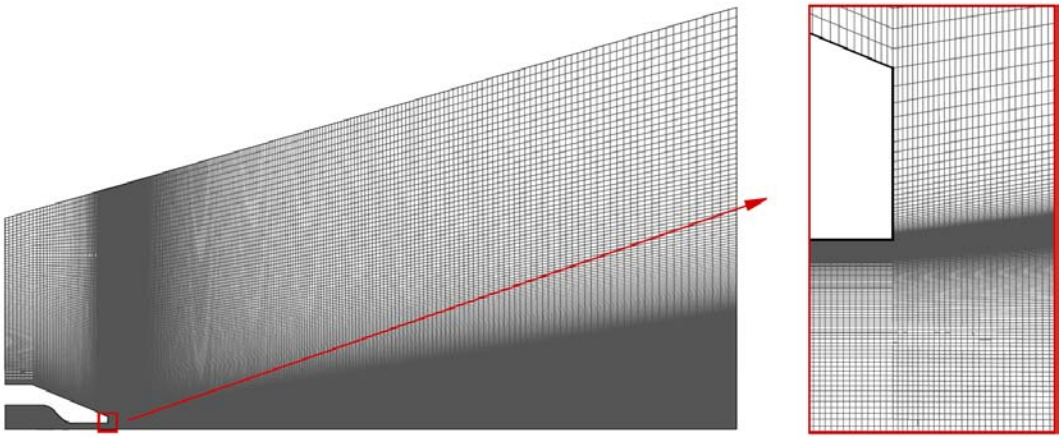

Figure 5: Mesh of subsonic nozzle

To determine the discretization error, a grid independency study using three different grid sizes of approx. 75,000, 150,000 and 290,000 grid cells was performed. The obtained results showed no significant difference.

RESULTS

The boundary conditions for the free jet are the pressures at the nozzle inlet and exit, total temperature and ambient temperature. The exit pressure is in our case equal to the ambient (barometric) pressure. In Table 1 the boundary conditions of the investigated cases are summarized.

Table 1: Boundary conditions for the tested free jets

free jet	p_{inflow} [bar]	T_{inflow} [K]	p_{∞} [bar]	T_{∞} [K]
subsonic	1.76	292	0.96	292
supersonic	3.524	292	0.96	290
supersonic	3.538	550	0.964	291

The used coordinate system and the investigated planes are shown for the subsonic nozzle in Figure 6.

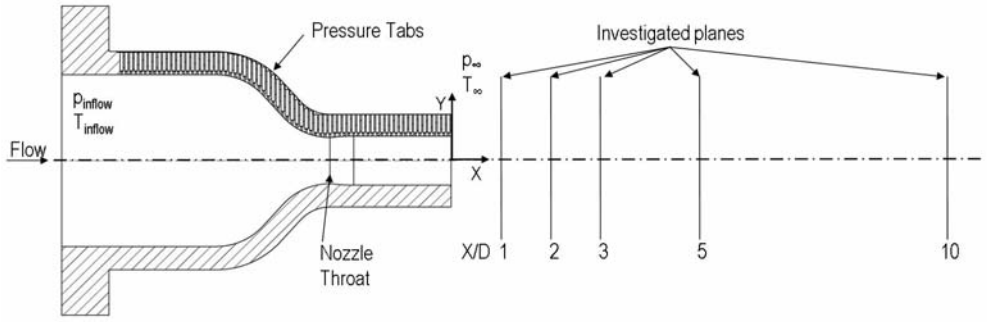

Figure 6: Subsonic nozzle with used coordinate system and investigated planes

The static pressure at the exit of the nozzle defines the flow form in the nozzle and free jet. At (relatively) high pressure ratios p_{∞}/p_0 (dependent on contraction ratio A_{exit}/A^*) a normal shock appears downstream of the throat which creates a subsonic flow. The shock also adjusts the static pressure at the nozzle exit to the ambient pressure. As the pressure ratio is lowered the shock moves downstream until it appears at the nozzle exit. This phenomenon is shown in Figure 7.

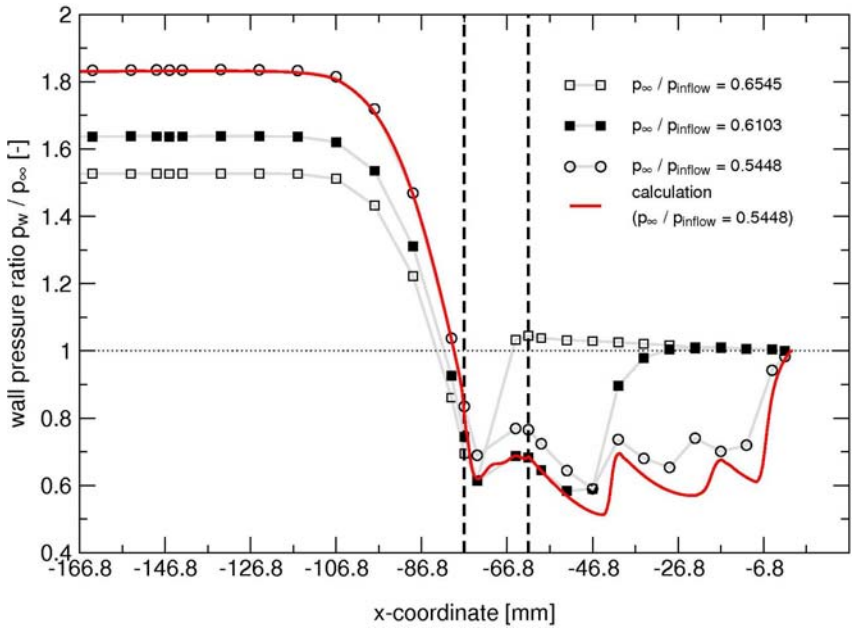

Figure 7: Normalized wall pressure distribution p_{∞}/p_0 in a convergent-divergent nozzle for subsonic free jets

The dimensionless wall pressure distribution inside the subsonic nozzle is plotted over the axial distance along the nozzle for three different pressure ratios. The two dashed lines mark the throat and the beginning of the constant cross section (corresponding to Figure 2). The above mentioned normal shock is recognizable by the abrupt wall pressure increase. The shock system that is visible upstream the normal shock (especially for $p_\infty/p_0 = 0.5448$) is due to a non matched nozzle. The flow for the lowest pressure ratio was numerically simulated. The result is also presented in Figure 7. It is visible that after the throat the wall pressure is predicted lower and the position of the last reflected shock is predicted further downstream.
We simulated the nozzle flow with different turbulence models. No significant influence on the wall pressure distribution could be found. A reason for the shock displacement is probably due to uncertainties in the boundary layer simulation.

Measurements were taken at the five different planes show in Figure 6. The subsonic nozzle exit diameter is D = 31.4 mm.
In Figure 8 the distribution of the Ma number in the subsonic free jet is plotted. The radial distance Y is normalized by the nozzle exit radius.

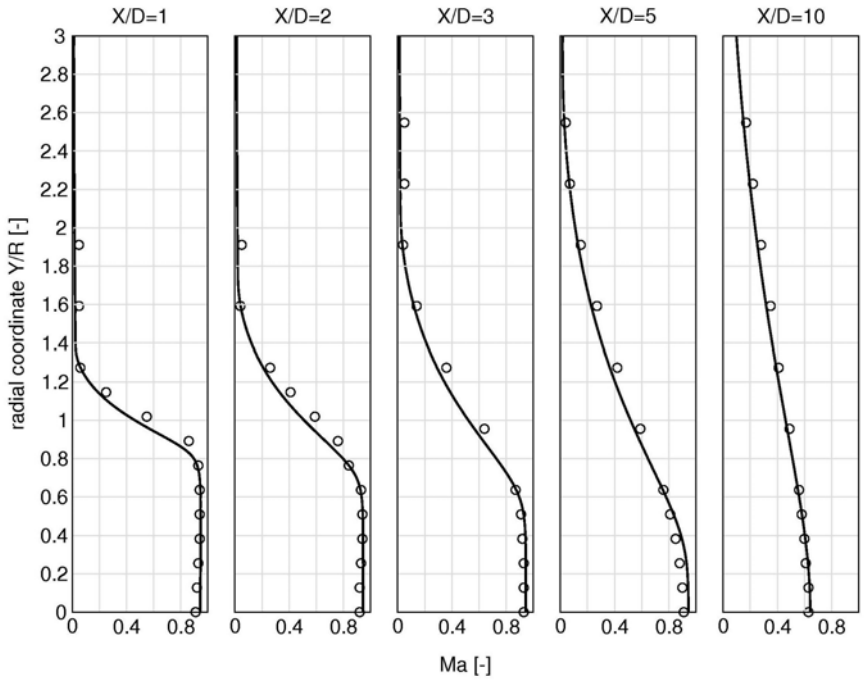

Figure 8: Ma distribution in a cold subsonic free jet (○) conventional probe measurement (-) calculation

In subsonic flows the total pressure is equal to the pitot pressure. Thus the Ma number is calculated with the measured pitot pressure p_{pitot} by [9]:

$$Ma = \sqrt{\frac{2}{\kappa - 1}\left[\left(\frac{p_{pitot}}{p_\infty}\right)^{\frac{\kappa-1}{\kappa}} - 1\right]}. \qquad \text{(Eq. 1)}$$

A good agreement between experimental data and numeric prediction is found. Only a very small deviation is visible in the shear layer.
The radial profiles of the normalized static temperature T/T_∞ and normalized speed of sound a/a_∞ are presented in Figure 9.

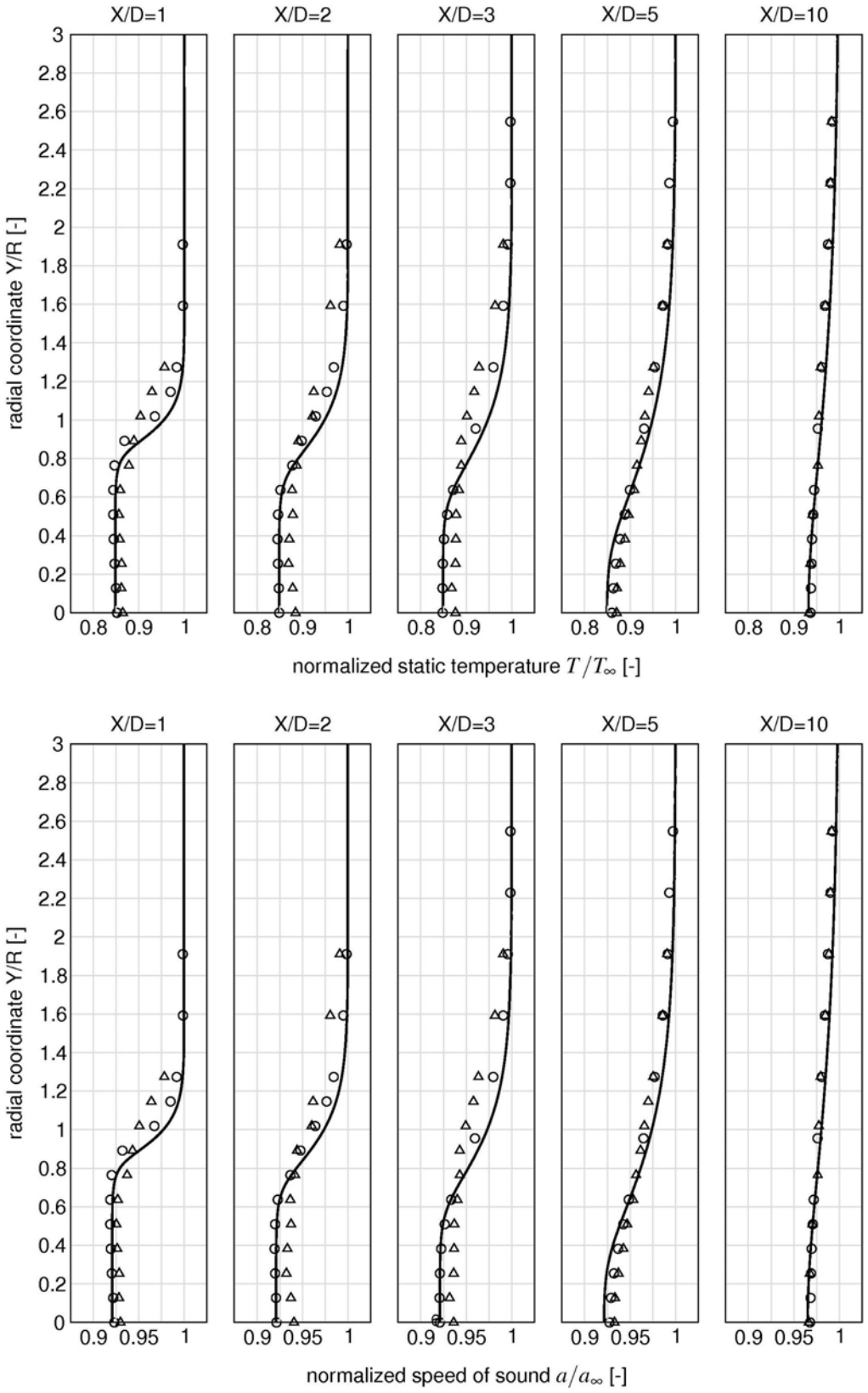

Figure 9: normalized static temperature and speed of sound in a subsonic free jet
(○) conventional measurement (△) LITA (-) calculation

Very good agreement between conventional diagnostic techniques and numeric prediction is found, whereas the results of LITA measurement show a small deviation. This deviation is visible especially in the

planes near the nozzle exit. However the deviation is in the range of the measuring accuracy (4.6 % for static temperature and 2.3 % for speed of sound).

The supersonic nozzle is operated at matched conditions for different total temperatures. In Table 2 the positions of the investigated planes are summarized. The coordinate system and the position of the investigated planes correspond to the ones shown in Figure 6.

Table 2: Investigated planes within the subsonic free jet

Plane	1	2	3	4	5
X-Position [mm]	32.18	64.36	96.55	160.91	321.83
X/D [-]	1	2	3	5	10

In Figure 10 the distribution of the Ma number in the cold and hot supersonic free jet is presented. The Ma number is calculated with the Pitot-Rayleigh-Equation [9]:

$$\frac{p_{pitot}}{p_{\infty}} = \left(\frac{\kappa+1}{2}Ma^2\right)^{\frac{\kappa}{\kappa-1}} \left(\frac{2\kappa}{\kappa+1}Ma^2 - \frac{\kappa-1}{\kappa+1}\right)^{\frac{1}{1-\kappa}}. \qquad \text{(Eq. 2)}$$

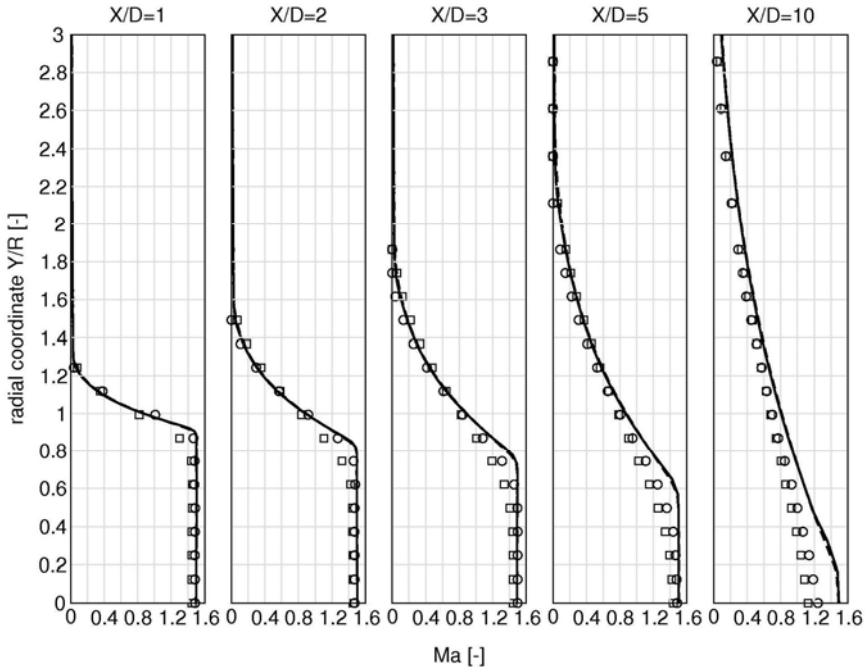

Figure 10: Ma distribution in a cold and hot supersonic free jet at matched condition
cold: (○) conventional probe measurement (-) calculation
hot: (□) conventional probe measurement (--) calculation

The numeric predictions show no significant dependency on the inflow temperature, whereas a small dependency exists in the experimental results. It is obvious especially in the shear layer.
Radial profiles of the normalized static temperature T/T_∞ and normalized speed of sound a/a_∞ are presented in Figure 11. Good agreement between the results is found. As in the distribution of the Ma number, a small difference between experimental and numerical data is visible in the shear layer. It is also visible that the length of the potential core is predicted longer. This phenomenon is due to the constants in the turbulence model [10]. As we wanted to compare the results with the standard turbulence model we did not fit the constants to our experimental setup.

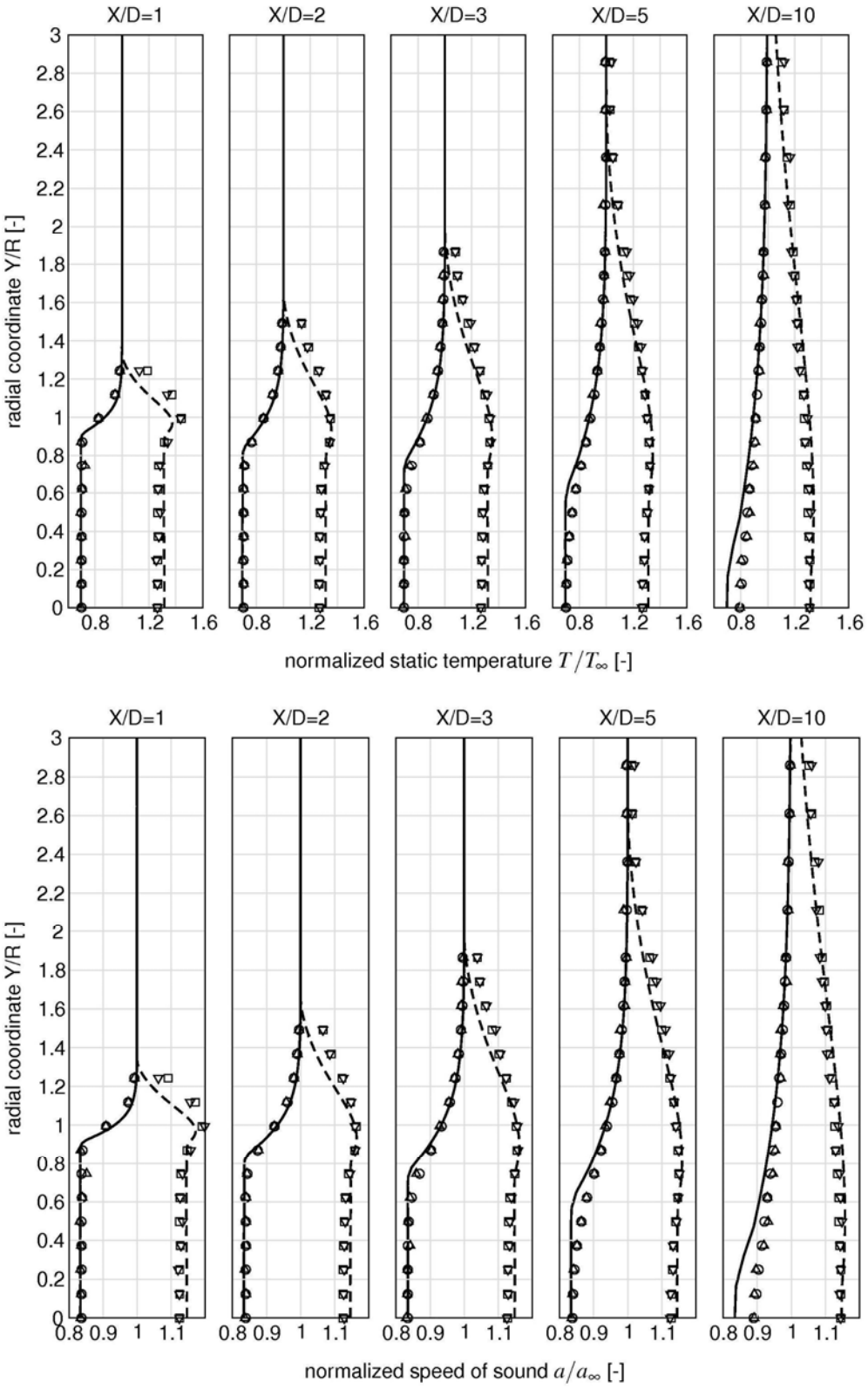

Figure 11: normalized static temperature and speed of sound in a cold and hot supersonic free jet at matched condition
cold: (○) conventional probe measurement (-) calculation (△) LITA
hot: (□) conventional probe measurement (--) calculation (▽) LITA

CONCLUSION

In this experimental and numerical study we investigated subsonic and supersonic free jets at different total temperatures of up to 550 K. For the experimental investigations we used conventional probe measurement (pitot pressure probe and total temperature probe) and the nonintrusive measurement technique LITA. Experimental results for profiles of the static temperature and speed of sound at various downstream locations are compared for the different cases. The comparison showed in general a very good agreement between the different measurement techniques. Only for the subsonic free jet, especially in the shear layer, small deviations are found. However these deviations are within the measuring accuracy (4.6 % for static temperature and 2.3 % for speed of sound).
For the comparison between experiment and numerical prediction we compared Ma number, static temperature and speed of sound profiles at different measurement planes within the free jet and the wall pressure distribution inside the subsonic nozzle. In general a good agreement was found.
The performed study proved the reliability of LITA measurements in highly turbulent supersonic free jets. For the future investigations of mixing free jets and hot reacting free jets are planned.

ACKNOWLEDGEMENT

This work was performed at the Graduate School 'Aerothermodynamic Design of a Scramjet Propulsion System for Future Space Transport Vehicles' (GRK1095/1). The authors would like to thank the German Research Foundation (Deutsche Forschungsgemeinschaft) for its financial support.

REFERENCES

[1] J. M. Eggers. *Velocity profiles and eddy viscosity distributions downstream of a Mach 2.22 nozzle exhausting to quiescent air*. NASA TN D-3601, September 1966.
[2] J. Panda and R. G. Seasholtz. Measurement of shock structure and shock-vortex interaction in underexpanded jets using Rayleigh scattering. *Physics of Fluid*, 11(12):3761 – 3777, 1999.
[3] R. G. Seasholtz, J. Panda, and K. A. Elam. Rayleigh scattering diagnostic for measurement of velocity and density fluctuation spectra. AIAA paper 2002-0827, 2002.
[4] Anderson, J. D. Jr.: *Modern Compressible Flow With Historical Perspective.* Third Edition. McGraw-Hill, 2004
[5] Cummings, E.B., Laser-induced thermal acoustics: simple accurate gas measurements, *Optics Letters* 19 (1994), No. 17, pp. 1361-1363.
[6] Cummings, E.B., Leyva, I.A., Hornung, H.G., Laser-induced thermal acoustics (LITA) signals from finite beams, *Applied Optics* 34 (1995), No. 18, pp. 3290–3302.
[7] Schlamp, S., Cummings, E.B., Hornung, H.G., Beam misalignments and fluid velocities in laser-induced thermal acoustics, *Applied Optics* 38 (1999), No. 27, pp. 5724–5733.
[8] Schlamp, S., Sobota, T.H., Measuring concentrations with laser-induced thermalization and electrostriction gratings, *Experiments in Fluids* 32 (2002), No. 6, pp. 683–688.
[9] Shapiro, A. H.: *The Dynamics and Thermodynamics of Compressible Fluid Flow.* Bd. I. The Ronald Press Company New York, 1953
[10] Pope, S. B.: An Explanation of the Turbulent Round-Jet/Plane-Jet Anomaly. In: *AIAA Journal* 16 (1978), Nr. 3, S. 279–281